X-Ray absorption spectroscopy to study metallic clusters†

Agnès Traverse*

LURE, (CNRS UMR 130), Bâtiment 209A, Université de Paris-Sud, 91405 Orsay cédex, France

Metallic clusters are of considerable interest both from fundamental and technological points of view. A thorough understanding of their structure is a prerequisite to interpreting their physical and chemical properties. The basic concepts of X-ray absorption spectroscopy are recalled here in order to show what kind of information can be provided by this tool. Some results collected from the literature are presented concerning crystallographic structure, lattice parameters and the size of clusters. The importance of X-ray magnetic circular dichroism is also illustrated.

Clusters are objects made of a few atoms to a few hundred atoms. They are of great interest both from fundamental and technological points of view. Among the new and attractive fundamental properties, we can mention the increase in the magnetic moments observed either in a beam of clusters[1] or in clusters embedded in a polymer matrix[2] and the existence of giant magnetoresistance.[3] The activity around metal clusters is also motivated by technological applications in heterogeneous catalysis and magnetic recording and their tribological and optical properties.

Several techniques are used to prepare metallic clusters. Laser vaporization sources deliver cluster beams that can be studied while they fly[1] or that can be deposited on substrates, which can then be coated by an evaporated layer in order to protect them from oxidation.[4] The gas-aggregation technique consists in evaporating metallic atoms in an Ar atmosphere; the clusters are transported by the gas stream to a liquid helium cryopump where the gas is condensed.[5] Clusters embedded in a matrix can be prepared in the following ways: co-deposition by sputtering or electron evaporation on a substrate of two immiscible metals[6] or ion implantation of immiscible impurities in a target.[7] Chemistry techniques using microemulsions allowed experimentalists to produce small metallic particles embedded in polymers or metallic matrices.[8]

Determination of the structure of small metal clusters is of fundamental importance for correlation with their physical properties. The most significant questions concern atomic arrangement, crystallographic structure, lattice parameter and size. Cluster formation and growth processes are also of importance. A way to obtain this information is to submit them to the bright X-ray photon beam delivered by a synchrotron and to perform X-ray absorption spectroscopy (XAS). With this technique it is possible to measure their structural parameters, to determine the average size and to look at their electronic and magnetic properties.

Although in previous years, XAS, and more particularly the oscillations superimposed on the absorption coefficient, named extended X-ray absorption fine structure (EXAFS), have already been used to study metal clusters, especially in the field of catalysis (see for example ref. 9). Pettifer,[10] in a 1986 review article entitled 'X-ray absorption spectroscopy applied to metal clusters', concluded that 'for the present, those involved in applications of EXAFS will have to appreciate the limitations imposed by the lack of development in the basic experimental and theoretical physics necessary for this spectroscopy.' In the years following this article, a large amount of experimental and theoretical work has been performed and it is worthwhile to summarize 12 years later the results brought by XAS on metal clusters.

Although XAS sometimes appears difficult to operate, it is the goal of this paper to show its importance in the study of metal clusters. As catalysis research, which involves cluster characterization, is a wide field with its own literature, we will not mention results in this area, except very occasionally. We will restrict ourselves to metallic clusters and to particles whose diameters are in the 0.5 to 10 nm range. The purpose of this review is to show the value of XAS but not to present an exhaustive bibliography.

This paper is organized as follows: we first recall some elements of XAS from the theoretical point of view and from the experimental one. Then we report several results found in the literature concerning the formation and growth of clusters and their structural, electronic and magnetic properties.

X-Ray Absorption Spectroscopy

Because X-ray photons interact with electrons, they can probe the electronic properties of a material. As the photon wavelengths are of the order of interatomic distances, investigation of the local environment around a given type of atom in a composite matrix is possible, in terms of type, number of neighbors and distances. This structural information can be obtained for samples with specific short-range order, which could be the case in small clusters. Information about the oxidation state, the symmetry of the local environment and the partial density of unoccupied electronic states is also available.

The basic process, which has often been described in textbooks,[11] is the following. A photon beam with an intensity I_0 and a varying incident energy E is sent onto a specimen. The intensity transmitted through the sample, I_1, displays sharp jumps, occurring at specific energies, depending on the nature of the atoms present in the material. These jumps correspond to the absorption of a photon by a core electron, either s, p or d, leading to a loss of intensity of the incident beam. They take place when the photon incident energy matches the binding energy of the core electron. The fact that the absorption thresholds occur at precise energies dependent on the nature of the atom provides the atomic selectivity of the technique. When the X-ray energy becomes a little higher than the binding energy of a core electron, this one jumps to empty electronic states. The recorded intensity up to some 50 eV above the absorption edge is related to the partial density of unoccupied electronic states. This energy range is called the

* E-mail: traverse@lure.u-psud.fr

† Non-SI unit employed: $\mu_B \approx 9.27 \times 10^{-24}$ J T^{-1}.

X-ray absorption near edge structure (XANES). If the absorbed energy is increased, the electron is ejected into the vacuum. It can be represented by an emitted electron wave, which will be backscattered by the neighbors. The interaction between the emitted and the backscattered wave gives rise to interferences, whose intensity is related to the nature and number of neighbors and to the disorder, whereas the frequency is correlated to the distances between the photoabsorber atom and its neighbors. This energy range from 50 to 2000 eV above the absorption edge (when low noise data are collected) is called the EXAFS region.

The continuous nature of the X-ray energy spectrum and the high flux emitted by synchrotron rings, together with the polarization of the beam, have induced a widespread development of the XAS technique in various fields, including that of cluster research. Several review papers have already been published on XAS spectroscopy.[12–14]

In the next paragraph, the principle of XAS is briefly presented. In the following paragraphs, some indications are given on treatment of the XAS spectrum and on experimental details.

Principles

The X-ray absorption coefficient, $\mu_i(E)$, where E is the energy of the incident photon, due to excitation of an electron from a core level i to a final state f, is described in the dipole approximation by[11]

$$\mu_i(E) = (4\pi^2/\Omega)\alpha E \sum_f |\langle\psi_i|\hat{\boldsymbol{e}}\cdot\hat{\boldsymbol{r}}|\psi_f\rangle^2\delta(E - E_f + E_i)| \quad (1)$$

where E_1 and E_f are the energies of the initial and final states, respectively, Ω is the unit cell volume, $\alpha = 2\pi e^2/hc$ and $\hat{\boldsymbol{e}}$ is the polarization vector of the incident photon; $\hat{\boldsymbol{r}}$ is the vector between the absorber and the backscatterer.

The dipolar operator is odd, thus we have

$$\hat{\boldsymbol{e}}\hat{\boldsymbol{r}} = \sqrt{\frac{4\pi}{3}}\, Y_1^0(\theta, \phi) \quad (2)$$

in the case of linear polarization of the beam.

The Wigner–Eckart theorem, which contains the composition rules for spherical harmonics, leads to the following selection rules: $\Delta l = \pm 1$, $\Delta j = \pm 1$, $\Delta s = 0$ and $\Delta m = 0$. This means that an excited 1s core electron is sent to empty p states, or that a 2p core electron is excited to either an empty d state or an empty s state.

The core initial state is described by the wave function ψ_i. The problem is to evaluate the wave function corresponding to the final states ψ_f. Two approaches are possible:

(*i*) the band structure approach, which requires the structural and chemical periodicity of the material, and often time-consuming calculations, and

(*ii*) the scattering formalism, more adapted to clusters, which are often disordered and do not display long-range order. It is in this formalism that the oscillations are described.

One generally considers as a first approximation that the electronic mean free path is such that only one backscattering process towards the central atom from the neighboring ones takes place, or that only two atoms are involved. Taking into account two correction terms, namely (*i*) effects due to lattice vibrations (hence correlated to the sample temperature) and to structural disorder and (*ii*) inelastic losses inducing a modification of the wave vector k, the expression of the oscillations is given by[11]

$$k\chi(k) = \sum_j \frac{N_j}{r_j^2} |f_j(k, \pi)| \sin[2kr_j + \phi_j(k)] e^{-2\sigma_j^2 k^2} e^{-2r_j/\lambda_j(k)} \quad (3)$$

The wave vector (in $Å^{-1}$) is deduced from the energy E given in eV by

$$k = [(8\pi^2 m/h^2)(E - E_0)]^{\frac{1}{2}} = 0.5123(E - E_0)^{\frac{1}{2}} \quad (4)$$

where f_j is the probability of scattering at 180° by the atom j located on shell j at distance r_j from the absorber. There are N_j neighbors in this shell. ϕ_j is the phase shift due to the nature of both the absorbing and scattering atoms. The first correction term contains the Debye–Waller factor σ_j, which is a measure of the structural and thermal disorders. The second correction term contains the mean free path of the photoelectrons, λ_j.

In the energy range from 50 eV up to 1000–2000 eV above the edge, where the mean free path of the ejected electron is short, a single scattering approach is often considered as sufficient. Nevertheless, the importance of multiple scattering contributions for all signals corresponding to shells above the first is now well-recognized.

Data treatment

The XANES parts of the recorded spectra are usually interpreted *via* comparison with standard samples or amongst different samples. To perform these comparisons, the spectra are background subtracted, then normalized to one for an energy value located about 50–100 eV beyond the edge.

The EXAFS oscillations must be extracted from the absorption spectrum $\mu(E)$. The successive steps are: (*i*) subtraction of a pre-absorption background due to other absorption processes occurring in the target and (*ii*) subtraction of the atomic absorption term, $\mu_0(E)$; the one observed if the absorbers are not surrounded by other atoms. It is usually approximated by a polynomial function. Then the EXAFS $\chi(E)$ is given by

$$\chi(E) = [\mu(E) - \mu_0(E)]/\mu_0(E) \quad (5)$$

The experimental spectrum is then converted to a k scale and a Fourier transform is calculated in order to obtain peaks corresponding to the positions r_j where neighboring shells are located.

Features present in both XANES and EXAFS spectra, and consequently in Fourier transforms, are dependent on the local atomic arrangement around the photo absorber. For example, fcc and bcc crystals display a two-peak and a one-peak feature, respectively, in the XANES spectra, whereas the peak intensities and shape in the Fourier transforms are different in the range of 0.2 to 0.6 nm. See the example of Cu and Fe in Fig. 1. In principle, a careful observation of these features might help in the crystallographic structure determination of the clusters.

The Fourier transform can be viewed as a pseudoradial function (PRF). Under some conditions it is possible to identify the neighboring atoms of the absorber. For example, a shell of light atoms surrounding the absorber will add a contribution at short distance, as seen in Fig. 2, which compares the Fourier transforms of pure Ti and of TiN.

To obtain quantitative information on the local environment, that is the number of neighbors in a given shell and its distance from the absorbing atom, the peak of interest is selected and an inverse Fourier transform is calculated. By a fitting procedure, f and ϕ being known for this specific absorber-backscatterer combination, N and r can be deduced. Several software packages have been written to perform this data treatment.[15] The first peak in the Fourier transform due to the closest shell results evidently from a single scattering process. Hence, the corresponding oscillation can be treated in this framework.

One problem is to know f, the backscattering probability, and ϕ, the phase shift. They can be deduced either from well-known standard samples or taken from the tables of McKale[16] or Teo and Lee,[17] for example, which consider a single scattering process only. Several codes, such as FEFF,[18]

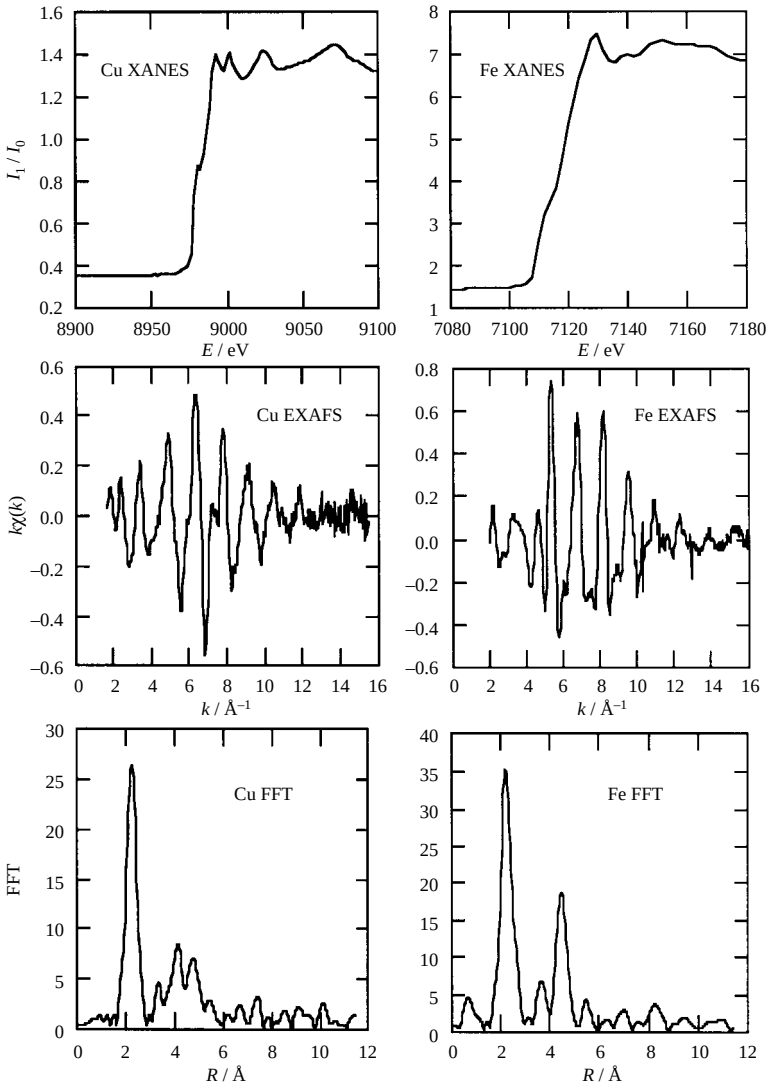

Fig. 1 XANES, EXAFS and Fourier transform of bulk fcc Cu and bcc Fe

CONTINUUM,[19] or GNXAS,[20] take into account the multi-scattering processes and provide these phase and amplitude files. They also allow the *ab initio* calculation of the whole absorption spectrum and oscillations.

The average coordination number is smaller for clusters than for corresponding bulk material. This comes from the fact that atoms at the cluster surface have fewer neighbors than those located in the core of the cluster. Therefore, there is a relationship between the average number of neighbors and the cluster size. The mean cluster diameter can be estimated by comparing the measured N value with that calculated for a given cluster size, assuming a given crystallographic structure. This was studied by Greegor and Lytle in 1980.[21] In a more recent work,[22] a formula was derived for spherical clusters with only one type of atom, relating the average number of neighbors in a given coordination shell deduced from the experimental oscillation simulation and the average diameter:

$$\langle N_{\mathrm{red}}(\rho)\rangle = 1 - \tfrac{3}{4}\rho + \tfrac{1}{16}\rho^3 \qquad (6)$$

where $\langle N_{\mathrm{red}}\rangle$ is the average number of neighbors normalized to unity, hence $\langle N_{\mathrm{red}}\rangle = \langle N\rangle / N_i$ with N_i the number of neighbors in the infinite lattice for the ith coordination shell located at R_i. ρ is equal to $2R_i/D$ where D is the diameter of the cluster. In Fig. 3 we notice that $\langle N_{\mathrm{red}}\rangle$ is equal to 0.3 for clusters of 0.5 nm diameter if R is 0.25 nm.

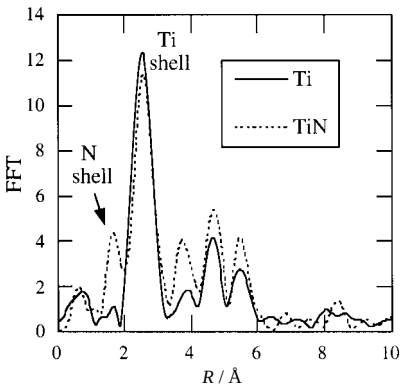

Fig. 2 Fourier transform of bulk hcp Ti and fcc TiN

Experimental conditions

In XAS experiments, a standard measurement consists in measuring (*i*) a current proportional to the number of photons incident on the sample and (*ii*) a current proportional to the number of photons transmitted by the sample if working in the transmission mode. However, both fluorescence emission (more probable for $Z > 30$) and secondary electron emission (more probable for $Z < 30$) take place from the surface of the specimen. They result from the deexcitation of the absorber and are correlated to the photon absorption process. The escape depth for electrons is of the order of 10 to 100 nm and

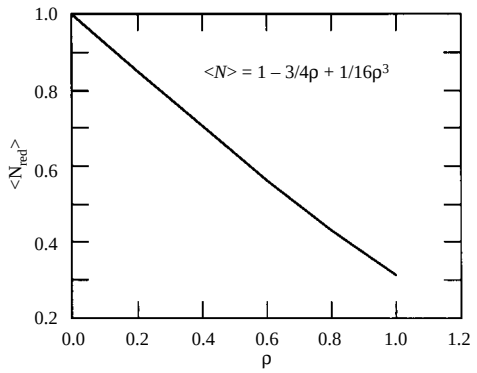

Fig. 3 $\langle N_{red} \rangle$ *vs.* the reduced diameter. (Reproduced from ref. 22 with permission of les Editions de Physique)

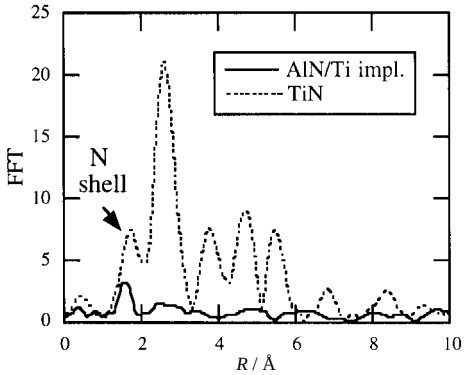

Fig. 4 Comparison between the Fourier transform of Ti implanted in AlN and TiN. The peak corresponding to an N shell is clearly visible at small distances. (Reproduced from ref. 24 with permission of the Institute of Physics, Warsaw)

of a few microns for the fluorescence photons. In total electron yield (TEY) detection mode, concentrations of a few atomic percent are required whereas in fluorescence mode, concentrations 10 and even 100 times lower can be achieved. Of course these detection limits also depend on the photon flux and on the performances of the detector. These modes are often well-adapted to experiments performed on clusters deposited on substrates or embedded in a matrix. Better signals are recorded when experiments are performed at liquid nitrogen temperature.[23]

The photon or electron yield is recorded while the monochromator scans the energy of the incident photon beam from E_1 (about 200 eV below the absorption edge E_0) to E_2 (some 1000 to 2000 eV above E_0). Experiments are often performed at the K edge of transition metals such as Cu, Ni, Fe and Co and at the L edges of high Z elements such as Au, Pt, Ir, Os, *etc.*

Cluster Analysis

In this paragraph we now give some examples of results concerning clusters studied by XAS.

Formation and growth processes

Formation process. The first example concerns metallic atoms, Ti and Cu, implanted in a ceramic, AlN. By comparing the Fourier transform of the signal for a bulk metal with that corresponding to the implanted atoms, it was possible to reveal the formation of cluster. In Fig. 4 it is clear that the Fourier transform of Ti implanted in AlN indicates the presence of an N shell around Ti.[24] In Fig. 5 Fourier transforms for different Cu concentrations implanted in AlN indicate a Cu surrounding very similar to that of bulk Cu.[7] We concluded that Ti was surrounded on average by four nitrogen atoms (thus it is substituted for Al in the AlN matrix) whereas Cu formed clusters. The heat of formation of TiN is -80.4 kcal mol^{-1}; that of CuN is $+17.8$ kcal mol^{-1}. This means that Ti—N bonds are thermodynamically favoured and Cu—N bonds are not. This thermodynamics argument allows us to understand, in this particular case, the cluster formation. As Ni—N bonds are not thermodynamically favoured, Ni clusters are also formed by implantation in AlN.[25]

By analysing the first peak in the Fourier transform, it was possible to follow the formation steps of the Ni clusters with annealing temperature[26] in the case of $Ni_{0.20}Ag_{0.80}$ alloys prepared by DC magnetron sputtering. Up to 250 °C annealing, two phases are present: a Ni phase, where the Ni atoms are mainly in small, poorly ordered agglomerates, and a Ag-rich phase, where some Ni atoms occupy substitutional sites in the Ag matrix. After annealing at 250 °C for 10 min, the cluster diameters increase and 40% to 50% of the Ni is in the form of clusters. After annealing at 400 °C for 10 min, the nanostructures evolve towards larger, well-ordered particles while the Ag-rich phase is Ni impoverished. A slightly different evolution is observed in Co_xAg_{1-x} alloys prepared under similar conditions.[27]

Growth process. Cu atoms were deposited with the help of a Knudsen cell, calibrated using a quartz oscillator on an alumina surface, with which they were proved weakly to interact. The average diameter of the particles in the 0.5 to 1.4 nm range can be followed with deposition time *via* the average number of neighbors deduced from a simulation of the first peak in the Fourier transform. The result is a scaling law characteristic of a coalescence process (Fig. 6).[28] A coalescence process was also found for laser-evaporated clusters on a glass substrate using transmission electron microscopy.[29]

Structural properties

Crystallographic structure. Small clusters in some cases display crystallographic structures different from the one of the corresponding bulk material.

Fe clusters prepared by the gas-aggregation technique display a bcc structure, as in the bulk, down to a mean diameter of 0.9 nm and an fcc- or hcp-like structure below this size.[30] Ag clusters larger than 1.2 nm mean diameter show a structure consistent with an fcc lattice. Smaller Ag clusters display a different structure, which was not identified in this article.[30]

Co clusters are found to be fcc when prepared either by laser evaporation[29] or by ion implantation, even up to diam-

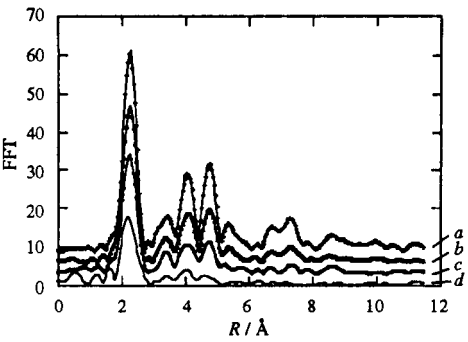

Fig. 5 Fourier transform for different sizes of Cu clusters. Curve *a* is bulk Cu; curves *b–d* are for 20%, 14% and 7%, respectively, of Cu implanted in AlN and annealed. (Reproduced from ref. 24 with permission of the Institute of Physics, Warsaw)

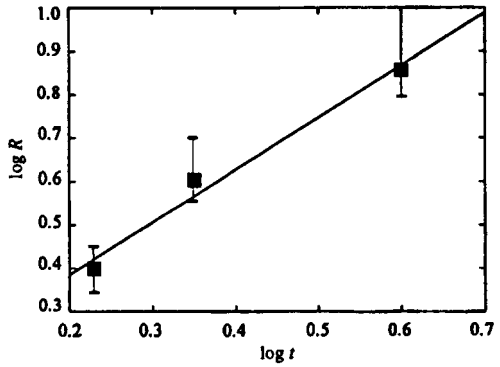

Fig. 6 Cluster radius R *vs.* time deposition on a logarithmic scale[28]; the slope = 1.2

eters as large as 9 nm, whereas Ni clusters were found to be fcc[25] in the diameter range of 0.9 to 4 nm.

Lattice parameters. Two different behaviors were observed concerning the lattice parameters. In some studies, it has been shown that the lattice parameter decreases for small size clusters whereas the reverse was also found.

In the case of Cu clusters isolated in solid Ar[31] and of Au clusters evaporated on polymer films,[32] a 2% to 2.5% reduction is measured for diameters of about 1 nm (see Fig. 7). Contractions as large as 4% and 8% were measured for Cu and Ni clusters, respectively, with a 1 nm diameter prepared by evaporation of metal and carbon layers on a polymer.[33] A larger contraction of 18% is observed for Fe clusters in solid neon,[34] but no relationship with the cluster diameter is given. Montano *et al.*[31] also obtained the same order of reduction for Cu_2 dimers.

An interpretation of the bond length contraction with decreasing cluster size is given by Apai *et al.*[33] as due to a redistribution of charge. The number of nearest-neighbor atoms at the cluster surface being less, there is a reduction in repulsive interactions between nonbonded electron pairs. Balerna *et al.*[32] invoke the surface stress due to the high value of the surface-to-volume ratio. They show that the bond length reduction is inversely proportional to the diameter D. This is also true in the liquid drop model where the contraction ΔR due to the surface stress f is proportional to $Kf(R_b/D)$. Here R_b is the metal bulk first neighbor distance and K the bulk compressibility.

For example, for the following clusters: Os, Pt and Ir deposited on SiO_2 and Ir on Al_2O_3, the interatomic distances are equal to those of the bulk within the experimental uncertainties.[9] In clusters produced by ion implantation,[24,25] the interatomic distances are also similar to those of the bulk within the experimental uncertainty.

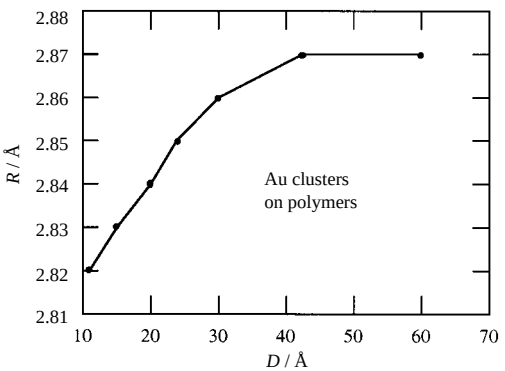

Fig. 7 Lattice parameter decrease for Au clusters deposited on polymers from ref. 32

The reason for such discrepancies is not clear. The precision with which the distance is measured, typically ± 0.002 nm and even less, does not allow us to doubt the announced reductions. We could have thought that clusters deposited on substrates, or flying, or embedded in a gas, display a bond length reduction due to the arguments presented above. This is not the case for the deposited clusters discussed in ref. 9. On the other hand, clusters in matrices cannot display this behavior since they are surrounded by atoms. Supplementary information on substrate–cluster and matrix–cluster interactions is required to help in explaining these different results.

Coordination numbers and average diameters. Equation 6 predicts a large reduction of the coordination number when the cluster size is reduced, as reported in Fig. 3. Such reductions were experimentally observed whatever the preparation technique.[9,24–28,32] An example of the reduction of the intensity of the Fourier transform peaks is seen in Fig. 5 for Cu clusters embedded in an AlN matrix, together with the N and D values presented in Table 1.

From the formula of ref. 22, the uncertainty in the radius r is given by $\Delta r/r = \Delta\langle N_{red}\rangle/(1 - \langle N_{red}\rangle)$. This means that an initial uncertainty of 5% in $\langle N_{red}\rangle$ gives a relative uncertainty in r of 10% if $\langle N_{red}\rangle = 0.5$, and of 25% if $\langle N_{red}\rangle = 0.8$. Hence XAS is more accurate in the determination of very small cluster sizes. One must note that the size distribution is not obtainable by XAS, yet it is often an important parameter in the discussion of physical properties.

The role of the Debye–Waller factor, σ, on the reduction of the EXAFS amplitude from which N is deduced must be mentioned. σ represents the thermal and structural disorders. Its role is not exactly similar in the sense that a reduction of N is more effective at low k values whereas a large σ is more effective at large k values. A discussion of the role of σ, for example on the defect concentration in ball-milled nanocrystalline iron, can be found in ref. 35. The authors show that the observed amplitude reduction can be interpreted by a large density of structural defects and not by a size decrease.

We meet here a limitation of the XAS technique and as discussed in ref. 36, it is necessary to have recourse to other techniques also available at synchrotron radiation facilities, such as anomalous small angle X-ray scattering (ASAXS) sometimes performed in grazing incidence (GISAXS). This was done for Co_xAg_{1-x} and heterogeneous alloys where Co and Ni form clusters.[37] The morphology and organization of Co clusters, prepared by evaporation of a Co and Al_2O_3 multilayered sample, has been obtained by GISAXS.[38] Furthermore, the correlations in the plane of the layers and the cross-correlations from layer to layer were determined by this technique.

Thermal properties

The amplitude and phase of EXAFS oscillations are influenced by both structural and thermal disorders. This sensitivity can be exploited to obtain quantitative information *via* the Debye–Waller factor on local vibrational dynamics in clusters. Note that it is rather easy to measure temperature-

Table 1 Cu concentrations of implanted and post-annealed samples, distance R to the first shell (uncertainty ± 0.002 nm), average coordination number N (uncertainty ± 0.1) in the first shell around Cu and average diameter D calculated with the formula in ref. 22

	Foil	20%, annealed	14%, annealed	7%, annealed
R/nm	0.255	0.255	0.255	0.253
N	12	10.7	9.9	6.9
D/nm		3.5	2.2	0.9

dependent EXAFS. By measuring the difference between oscillations at 300 and 80 K, it is possible to separate the thermal contribution from the structural one. This contribution is related to the Debye temperature, θ_D, of the cluster.

Balerna *et al.*[32] found a Debye temperature equal to 90% of the bulk one for Au clusters deposited on polymers with diameters between 2 and 4.25 nm. Reductions of 70% and 80% in θ_D were measured for Ag and Pd clusters, respectively, deposited on SiO_2 substrates with diameters smaller than 2 nm.[39] The decrease of θ_D is assigned to the existence of atoms located at the surface with higher mobility than those in the center.[32] Indeed, a reduction of θ_D of the same order of magnitude was predicted in ref. 40.

In the case of clusters embedded in the AlN matrix, prepared by ion implantation,[25] we measured similar Debye temperatures in the bulk and in the clusters. The discrepancy with the results presented above is only apparent. In fact for clusters embedded in matrices, one can argue that no atoms are really at the surface since they 'see' the host atoms, which might reduce their mobility.

Electronic properties

As mentioned above XANES is a picture of the empty electronic states, hence it contains information on the electronic properties of materials.

The bond length contraction observed in ref. 33 is strongly correlated to shifts measured in the K-edge threshold energy. These shifts, of the order of 0.7 eV in Cu and 1.3 eV in Ni, are indicative of core-level binding-energy shifts relative to the Fermi level caused by changes in the electronic configuration.

Deeper insight into the electronic distribution changes is provided by the features seen in the XANES spectrum. For example, at the Ni K edge the initial absorption rise comes from electronic states having an s–p–d admixed symmetry (A in Fig. 8), whereas the second absorption rise (B and C in Fig. 8) has the nearly pure 4p symmetry.[11]

In a small size cluster, modification of the hybridization is expected, which might be detected in the XANES features. An example is provided in Fig. 8 where the K edge of Ni clusters is compared to the one of bulk Ni. Feature A is smoothed and located at lower energy whereas features B and C are rounded. In Fig. 9 the edge of pure Cu is plotted together with the one of a 1 nm diameter cluster. A clear modification of the 4p empty states is also observed.[14,31]

Theoretical calculations of the electronic structure of small copper and nickel clusters were performed using the self-consistent-field Xα scattered-wave approach to molecular orbital theory.[41] It is interesting to see that for Cu, a_{1g} and t_u orbitals with s and p character, which are present above the

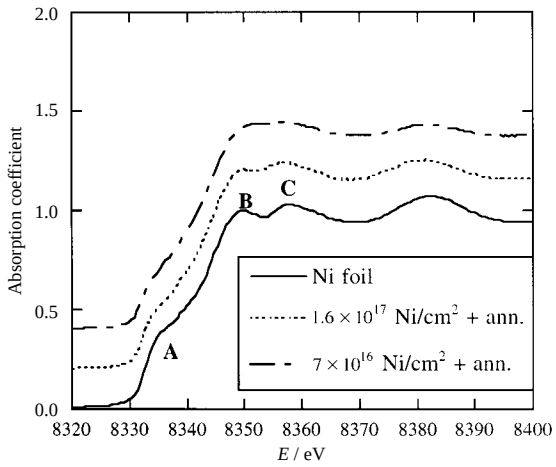

Fig. 8 XANES spectra for bulk Ni and 2.2 and 0.9 nm diameter Ni clusters

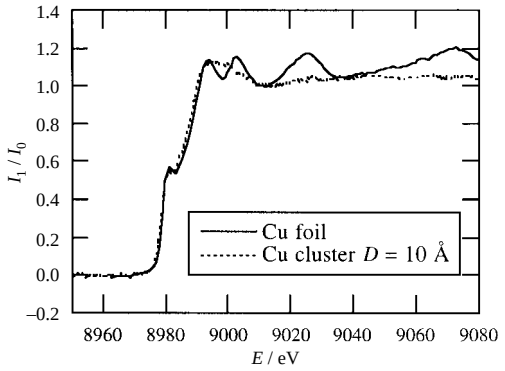

Fig. 9 XANES spectra for bulk Cu and a 1 nm diameter Cu cluster

Fermi level for Cu atoms located in the cluster core, do not occur for Cu atoms located at the cluster surface; this can qualitatively explain the observed modification in Fig. 9. For Ni atoms located at the cluster surface, a_{1u} orbitals with d character are located closer to the Fermi level than in the bulk, in qualitative agreement with the displacement of feature A observed in Fig. 8.

Looking at these features, we must underline that care has to be taken in deducing the crystallographic structure from them for very small sizes (*D* around 1 nm) since these features can be distorted in this particular case, as seen above.

Magnetic properties

X-Ray magnetic circular dichroism (XMCD) spectroscopy, first suggested by Erskine and Stern,[42] brings supplementary information not afforded by traditional magnetic techniques: the quantitative determination of spin and orbital magnetic moments for a specific atom in the sample. In ref. 43, one can find the basic concepts of XMCD spectroscopy. As magnetic properties of materials are mainly determined by their d electrons, these X-ray absorption experiments are performed at the $L_{2,3}$ edges, which contain the transitions from p to d electronic empty states.

To our knowledge very few articles exist on XMCD spectroscopy applied to metallic clusters. This might come from (*i*) the fact that this type of experiment is not very developed in general and (*ii*) the difficulty of the measurement itself, which requires a high flux of circularly polarized photons due to the small number of atoms inside the probed depth at these low energies, typically of the order of 2–3 nm.[43]

Zanghi and coworkers[44] compared the total magnetic moment measured by XMCD spectroscopy and by SQUID magnetometry at 300 and 100 K for Ni clusters of 300 atoms embedded in AlN. The good agreement between both measurements is very encouraging for this type of measurement. Moreover, it proves that the sum rules are applicable to clusters. The orbital magnetic contribution is still very small as compared to the spin magnetic contribution, evidence for crystal field effects as in bulk Ni. At 5 K, below the blocking temperature, the magnetic moment of this cluster is 0.6 μ_B, as in bulk Ni,[42] a value in agreement with the one in ref. 1 for a similar size.

In ref. 45, a very unusual behavior is reported. Co clusters were prepared by the gas-aggregation technique, then deposited on a Si substrate simultaneously with Cu atoms. XMCD measured at 300 K provides magnetic moment values dependent on the average cluster size but which are significantly less than that of a thin Co film, even for a cluster of 1000 atoms. Moreover, large values of the orbital to spin moments are observed. An interpretation is given in terms of a coupling between the clusters *via* a 'superexchange' mechanism.

Conclusion

X-Ray absorption spectroscopy is a local probe and thus appears to be a good tool to study metallic clusters whose dimensions are of the order of the probed range, that is a few angströms. Information around a given type of atom is provided thanks to its atomic selectivity. For about twenty years, XAS has been used to study either clusters embedded in gaseous or solid matrices and clusters deposited *in situ* on substrates. The cluster formation and growth can be checked by the analysis of the absorber environment. In principle, interactions between substrate and clusters or matrix and clusters can be investigated. It seems that few results exist in this area although they might help in the understanding of the different observed bond length behaviors. *Via* the measured coordination number, XAS appears suitable to deduce the size of small particles. It is easy to follow the EXAFS amplitude with temperature in order to obtain Debye temperatures, which provide information on lattice softening. Lastly, modifications in the XANES features inform us on the electronic redistributions expected in small size particles.

As with all techniques, XAS has its limitations and it is important to combine it with other techniques such as X-ray diffraction and small angle scattering, which provide information over a larger range than XAS.

We underline the development of X-ray magnetic circular dichroism spectroscopy in order to give us new microscopic insights into the magnetic behavior of these small objects.

Acknowledgements

I thank my colleagues for their comments and suggestions on this article: M. Borowski from ESRF, Grenoble, C. Hague from the Laboratoire de Chimie Physique, Paris, J. Mimault from the Laboratoire de Métallurgie Physique, Poitiers, C. Revenant from CEA, Grenoble and D. Zanghi from LURE, Orsay.

References

1 I. M. L. Billas, A. Châtelain and W. A. de Heer, *Science*, 1994, **265**, 1682.
2 M. Respaud, J. M. Broto, H. Rakoto, A. R. Fert, L. Thomas, B. Barbara, M. Verelst, E. Snoeck, P. Lecante, A. Mosset, J. Osuna, T. Ould Ely, C. Amiens and B. Chaudret, *Phys. Rev. B*, 1998, **57**, 2925.
3 S. R. Teixeira, B. Dieny, A. Chamberod, C. Cowache, S. Auffret, P. Auric, J. L. Rouvière, O. Redon and J. Pierre, *J. Phys.: Condens. Matter*, 1994, **6**, 5545.
4 M. Pellarin, B. Baguenard, J. L. Vialle, J. Lermé, M. Broyer, J. Miller and A. Perez, *Chem. Phys. Lett*., 1994, **217**, 349.
5 H. Abe, W. Schulze and B. Tesche, *Chem. Phys*., 1980, **47**, 95.
6 J. R. Regnard, J. Juanhuix, C. Brizard, B. Dieny, B. Mevel, J. Mimault and O. Proux, *Solid State Commun*., 1996, **5**, 4197.
7 A. Traverse, P. Parent, J. Mimault, S. Hagège and J. Du, *Nucl. Instrum. Methods B*, 1994, **84**, 204.
8 J. Osuna, D. de Caro, C. Amiens, B. Chaudret, A. Snoeck, M. Respaud, J. M. Broto and A. Fert, *J. Chem. Phys*., 1996, **100**, 35; A. Taleb, C. Petit and M. P. Pileni, *Chem. Mater*., 1997, **9**, 950; J. Rivas, R. D. Sánchez, A. Fondado, C. Izco, A. J. García-Bastida, J. García-Otero, J. Mira, D. Baldomir, A. González, I. Lado, M. A. López Quintela and S. B. Oseroff, *J. Appl. Phys*., 1994, **76**, 6564.
9 G. H. Via, J. H. Sinfelt and F. W. Lytle, *J. Chem. Phys*., 1979, **71**, 690.
10 R. F. Pettifer, in *Metal Clusters in Catalysis*, ed. B. C. Gates, L. Guczi and H. Konözinger, Elsevier, 1986, p. 231.
11 B. K. Agarwal, *X-Ray Spectroscopy, An Introduction*, 2nd edn., Springer Series in Optical Sciences, Springer Verlag, Berlin, 1991, vol. 15, ch. 7.
12 A. Fontaine, *Les Techniques de l'Ingénieur*, décembre 1988, p. 2698.
13 P. Lagarde, in *Initiation à la Spectroscopie d'Absorption des Rayons X*, ed. E. Prouzet and G. Ouvrard, Nantes, 1994.
14 A. Traverse, *J. Braz. Chem. Soc*., 1996, **7**, 199.
15 A. Michalowicz, *Logiciels pour la Chimie*, Société Française de Chimie, Paris, 1991, p. 102; A. San Miguel, *Physica B*, 1995, **208–209**, 177; C. Bouldin, L. Furenlid and T. Elam, *Physica B*, 1995, **208–209**, 190; A. Kuzmin, *Physica B*, 1995, **208–209**, 175.
16 A. G. McKale, *J. Am. Chem. Soc*., 1988, **110**, 3763.
17 B. K. Teo and P. A. Lee, *J. Am. Chem. Soc*., 1979, **101**, 2815.
18 J. J. Rehr and R. C. Alberts, *Phys. Rev. B*, 1990, **41**, 8139; M. Newville, B. Ravel, D. Haskel, J. J. Rehr, E. A. Stern and Y. Yacoby, *Physica B*, 1995, **208–209**, 154.
19 C. R. Natoli and M. Benfatto, in *EXAFS and Near Edge Structure IV*, ed. P. Lagarde, D. Raoux and J. Petiau, *J. Phys.* (*Paris*) *Colloq*., 1986, **47**, C8-11.
20 A. Filipponi, A. Di Cicco, T. A. Tyson and C. R. Natoli, *Solid State Commun*., 1991, **78**, 265; A. Di Cicco, *Physica B*, 1995, **208–209**, 125.
21 R. B. Greegor and F. W. Lytle, *J. Catal*., 1980, **63**, 476.
22 M. Borowski, *J. Phys. IV* (*Paris*), 1997, **7**, C2-259.
23 J. Mimault, J. J. Faix, T. Girardeau, M. Jaouen and G. Tourillon, *Meas. Sci. Technol*., 1994, **5**, 482.
24 M. Borowski, A. Traverse and J. Mimault, *Acta Phys. Pol. A*, 1994, **86**, 713.
25 A. Traverse, *Hyperfine Interactions*, 1997, **110**, 159.
26 C. Revenant-Brizard, J. R. Regnard, J. Mimault, O. Proux, B. Dieny and B. Mevel, *J. Phys. IV* (*Paris*), 1997, **7**, C2-1111.
27 J. R. Regnard, C. Revenant-Brizard, B. Dieny, B. Mevel and J. Mimault, *Mater. Res. Soc. Symp. Proc*., 1996, **400**, 329.
28 S. Gota, M. Gautier-Soyer, L. Douillard, J. P. Duraud and P. Le Fèvre, *J. Phys. IV* (*Paris*), 1997, **7**, C2-675.
29 J. Tuaillon, V. Dupuis, P. Mélinon, B. Prével, M. Treilleux, A. Pérez, M. Pellarin, J. L. Vialle and M. Broyer, *Philos. Mag. A*, 1997, **76**, 493.
30 P. A. Montano, J. Zhao, M. Ramanathan, G. K. Shenoy and W. Schulze, *Z. Phys. D*, 1989, **12**, 103.
31 P. A. Montano, G. K. Shenoy, E. E. Alp, W. Schulze and J. Urban, *Phys. Rev. Lett*., 1986, **56**, 2076.
32 A. Balerna, E. Bernieri, P. Picozzi, A. Reale, S. Santucci, E. Burattini and S. Mobilio, *Phys. Rev. B*, 1985, **31**, 5058.
33 G. Apai, J. F. Hamilton, J. Stohr and A. Thompson, *Phys. Rev. Lett*., 1979, **43**, 165.
34 H. Purdum, P. A. Montano, G. K. Shenoy and T. Morrison, *Phys. Rev. B*, 1982, **25**, 4412.
35 A. Di Cicco, M. Berrettoni, S. Stizza, E. Bonetti and G. Cocco, *Phys. Rev. B*, 1994, **59**, 12386.
36 D. C. Bazin, D. A. Sayers and J. J. Rehr, *J. Phys. Chem*., 1997, **101**, 11040.
37 C. Revenant, J. P. Simon, J. R. Regnard, I. Manzini and B. Rodmacq, *J. Appl. Crystallogr*., in press.
38 A. Naudon, D. Babonneau, F. Pétroff and A. Vaurès, *Thin Solid Films*, in press.
39 T. Yokoyama, S. Kimoto and T. Ohta, *Physica B*, 1989, **158**, 255.
40 M. Zhou and P. Sheng, *Phys. Rev. B*, 1991, **43**, 3460.
41 R. P. Messmer, S. K. Knudson, K. H. Johnson, J. B. Diamond and C. Y. Yang, *Phys. Rev. B*, 1976, **13**, 1396.
42 J. L. Erskine and E. A. Stern, *Phys. Rev. B*, 1975, **12**, 5016.
43 J. Stöhr and R. Nakajima, *J. Phys. IV* (*Paris*), 1997, **7**, C2-47.
44 D. Zanghi, C. Bellouard, H. Fischer, A. Traverse and G. Krill, *J. Phys.: Condens. Matter*, submitted.
45 D. A. Eastham, Y. Qiang, T. H. Maddock, J. Kraft, J.-P. Schille, G. S. Thompson and H. Haberland, *J. Phys.: Condens. Matter*, 1997, **9**, L497.

Received in Montpellier, France, 9th February 1998; *Paper* 8/01162A